http://dx.doi.org/10.1097/mm9.0000000000000006

MedMat

Original Research

OPEN

Active learning assisted piezoelectric materials synthesis on the basis of composite decision-making

En Zhao[a,b,c], Tingyu Wang[a], Yutong Wang[b], Fan Zeng[b], Ling Chen[b], Zhiyuan Zhu[b,*], Wei Tang[a,c,*]

Abstract

The synthesis and development of novel materials for soft electronics, health monitoring, etc, have become a research hotspot. Traditional laboratory synthesis is significantly time and resource consuming. Machine learning therefore becomes an ideal approach for expediting the experimental process, constructing a virtual and automated closed-loop material synthesis, and evaluation approach. In this work, we combined piezoelectric materials' synthesis with machine learning to achieve automatic design optimization. A total of 300 samples with different material recipes were used to train the initial active learning model. Thereafter, more samples were fabricated based on the recommended feasible recipes for each learning loop and then proceeded to the next round of learning. Through 10 active learning loops, 105 piezoelectric samples were stage-wise fabricated. Moreover, a reverse design model based on Bayesian optimization is demonstrated, and Spearman rank correlation coefficient and P values revealed the rules for the synthesis of piezoelectric materials. Finally, according to the setup model, we fabricate optimized piezoelectric materials and demonstrate their application in cycling monitoring. We anticipate this work establishes an essential approach to accelerate the development of new materials.

Keywords: Active learning, Cycling monitoring, Piezoelectric materials, Reverse design

1. Introduction

Flexible electronic devices, soft machinery,[1–3] have been widely developed, in recent. Therefore, more soft functional materials are required, and many researchers focus on the topic,[4–6] especially the synthesis of composite materials. Taking the flexible piezoelectric materials as an example, recent advancements involve incorporating ZnO, PZT, or $BaTiO_3$[7–9] into flexible substrates, such as polydimethylsiloxane (PDMS) or Ecoflex,[10–12] so as to obtain flexible piezoelectric materials. It serves important application scenarios such as smart medical treatment and life health.[13–18] However, traditional laboratory synthesis is definitely time and resource consuming. Thus, more intelligent approaches are needed. The rapidly advancing artificial intelligence (AI) technology is expected to provide solutions for this.

En Zhao, Tingyu Wang, and Yutong Wang contributed equally to this work.

[a]Beijing Institute of Nanoenergy and Nanosystems, Chinese Academy of Sciences, Beijing, China, [b]Chongqing Key Laboratory of Nonlinear Circuits and Intelligent Information Processing, College of Electronic and Information Engineering, Southwest University, Chongqing, China, [c]Institute of Applied Nanotechnology, Jiaxing, Zhejiang, China.

*Corresponding author: Address: Zhiyuan Zhu, Chongqing Key Laboratory of Nonlinear Circuits and Intelligent Information Processing, College of Electronic and Information Engineering, Southwest University, Chongqing, 4000715, China. E-mail address: zyuanzhu@swu.edu.cn (Z. Zhu); Wei Tang, Beijing Institute of Nanoenergy and Nanosystems, Chinese Academy of Sciences, Beijing, 101400, China. E-mail address: tangwei@binn.cas.cn (W. Tang).

MedMat (2024) 1:2

Received: 13 March 2024; Accepted 2 September 2024

Published online 25 September 2024

In the past, AI was used for material discovery,[19–22] structure optimization,[23,24] and performance prediction.[25–27] AI-driven autonomous experiments offer a novel paradigm for accelerating material research. However, one of the main challenges is to explore the huge design space of target properties that in the past relied on tremendous trial-and-error.[21,28] Williams et al[29] combined machine learning (ML) with elemental properties and material compositions to expand the search space and predict the performance of new catalysis materials, but it requires extra manual regulations for deep exploration. Active learning can navigate the design space iteratively, showing a promising solution for design space exploration.[21,30,31] Accordingly, various closed-loop material discovery approaches have been developed.[32–34] For instance, Kusne et al[22] utilized Bayesian active learning to predict phase-change materials, but the process lacks the real-time correction of experiments. Yang et al[30] employed active learning and data augmentation to achieve composite prediction of soft resistive materials, but the initial small sample number and insufficient richness of decision regression algorithms affected their exploration ability and prediction accuracy.[35,36]

Herein, we report an active learning model based on composite decision regression to investigate the synthesis of flexible piezoelectric materials. To ensure abundant initial space, 300 samples with different material recipes were fabricated under identical protocols. Then, we employed decision tree (DT), k-nearest neighbor algorithm (KNN), and random forest (RF) for composite decision regression, followed by space exploration. Afterwards, continuous iterative search begins, forming a closed-loop autonomous exploration, significantly accelerating the research of composite materials. Furthermore, we demonstrate that the reverse prediction model via Bayesian optimization can give out the optimal recipe according to the user's needs. Finally, we use cycling monitoring as an example to demonstrate the as-fabricated high-performance piezoelectric materials' applications.

2. Materials and methods

2.1 Materials

Polyvinyl alcohol (PVA, Aladdin, M_w=67,000), single-walled carbon nanotubes (SWCNT, Time-Nano, 1–2 nm), barium titanate ($BaTiO_3$, Aladdin, 99.9%), isopropanol (Aladdin, AR, ≥99.7%), and ethyl alcohol (Aladdin, AR, water ≤ 0.3%). Organic microporous filter membrane (JINTENG, 0.2 μm), VHB tape (3 M, 6 cm × 3 m), conductive silver paste (HumiSeal), and deionized water (Smart-Q15 water purification system, 18.2 MΩ cm).

2.2 Characterization

A field emission scanning electron microscope (SEM) was used to test and analyze the surface morphology and element distribution of PVA/SWCNT/$BaTiO_3$ piezoelectric nanocomposite material (pbs-PE material). X-ray photoelectron spectrometer (150 W, 650 μm) was used to perform X-ray photoelectron spectroscopy (XPS) tests and record X-ray photoelectron spectra. Raman spectrometers (laser: 633 nm, wave number range: 100–3500 cm^{-1}) were used to characterize the Raman spectra of the pbs-PE material and analyze the material composition. The charge, voltage, and current were measured with the Keithley 6514 electrometer. The maximum tensile strain of the pbs-PE material was measured by the linear testing machine (R-LP4).

2.3 Calculation of RMSE

For the active learning loop model, the prediction accuracy of sample performance is calculated by root mean square error (RMSE) defined in equation (1):

$$\mathrm{RMSE} = \sqrt{\frac{1}{N}\sum_{i=1}^{N}\left(\mathrm{prediction}^i - \mathrm{labels}^i\right)^2} \tag{1}$$

where N is the number of data in the test set; prediction labels based on test set data point i are represented by predictioni; labelsi is the actual label for data point i of the test set.

2.4 Experiment

2.4.1 Solution preparation

(1) Preparation of PVA solution: add 100 mg PVA to 100 mL deionized water, prepare 1 mg/mL solution through a magnetic stirrer (50°C), and then add deionized water to further adjust the solution concentration to 0.1 mg/mL. (2) Preparation of SWCNT dispersion: 100 mg SWCNT was added to 1000 mL isopropanol to prepare 0.1 mg/mL dispersion. (3) Preparation of $BaTiO_3$ solution: 100 mg $BaTiO_3$ is dissolved in 20 mL isopropanol and prepared into 5 mg/mL solution.

2.4.2 Preparation of sample

PVA and $BaTiO_3$ solutions were mixed with SWCNT dispersion at different mass ratios, and then the mixture was pumped on the microporous filter membrane by vacuum-assisted filtration device. The pbs-PE material was obtained after being fully dried in the vacuum drying chamber. Next, transfer the substrate and pbs-PE material to VHB tape, connect the copper wire to the pbs-PE material, and apply conductive silver adhesive to ensure good electrical contact. Finally, the PE layer is applied to the surface of the material (covering the entire material) to prepare piezoelectric nanogenerator (PENG) sensor.

2.5 Bayesian optimization

In the reverse design model based on Bayesian optimization, the loss function that evaluates the difference between the target performance and the predicted performance is defined by mean square error (MSE), as defined by equation (2):

$$\mathrm{MSE} = \frac{1}{N}\sum_{i=1}^{N}\left(\mathrm{prediction}^i - \mathrm{labels}^i\right)^2 \tag{2}$$

where N is the number of data in the test set; prediction labels based on test set data point i are represented by predictioni; labelsi is the actual label for data point i of the test set.

Bayesian optimization algorithm is based on expected improvement (EI) strategy. In Bayesian optimization, we need to make a trade-off between exploring the region of uncertainty and focusing on the region known to have a better target value. In order to effectively sample, the acquisition function is used to determine the next sampling location. Since EI will select the point with the greatest EI as the feature of the next query point, we choose it as the acquisition function. As shown in equation (3):

$$x_{i+1} = \mathrm{argmin}_x \mathrm{E}(||h_{i+1}(x) - f(x^*)|| \mid D_i) \tag{3}$$

where x is the position of the current point, $xi+_1$ is the position of the query point in step i + 1, f is the objective function (function to be optimized), and $hi+_1$ is the posterior mean of the proxy model in step i + 1. $D_i = \{(x_i,\ f(x_i))\}$, $\forall x \in x_{1:i}$ is the training data, and x^* is the actual position where f is maximized.

3. Results

3.1 Material synthesis and assembly characterization

By combining ML with experiments, a material discovery approach was reported to investigate the influence of varying material recipes on piezoelectric properties. Figure 1A illustrates the selection of 3 materials: PVA, $BaTiO_3$, and SWCNT. These materials were chosen to fabricate the flexible piezoelectric sensing material. To achieve this, we developed a 3-stage ML framework as depicted in Figure 1B. The framework encompassed materials characterization, space exploration, and reverse prediction.

The construction process of the piezoelectric sensing material incorporating PVA, $BaTiO_3$, and SWCNT is elucidated in Figure 2A. First, PVA, $BaTiO_3$, and SWCNT solutions are prepared and blended in precise proportions. Next, the mixture is deposited on the polycaprolactam (Nylon-6) microporous filter membrane through a vacuum-assisted filtration device, resulting in the creation of the pbs-PE material. Following that, the pbs-PE material was transferred to the substrate and wires were connected to assemble the PENG sensor. To assess the effective integration of the 3 materials, a series of characterizations were conducted. SEM images of the pbs-PE material are shown in Figure 2B and Supplementary Figure 1, http://links.lww.com/MEDMAT/A2, revealing interwoven SWCNT and uniformly distributed $BaTiO_3$ nanoparticles on the surface, providing preliminary evidence of

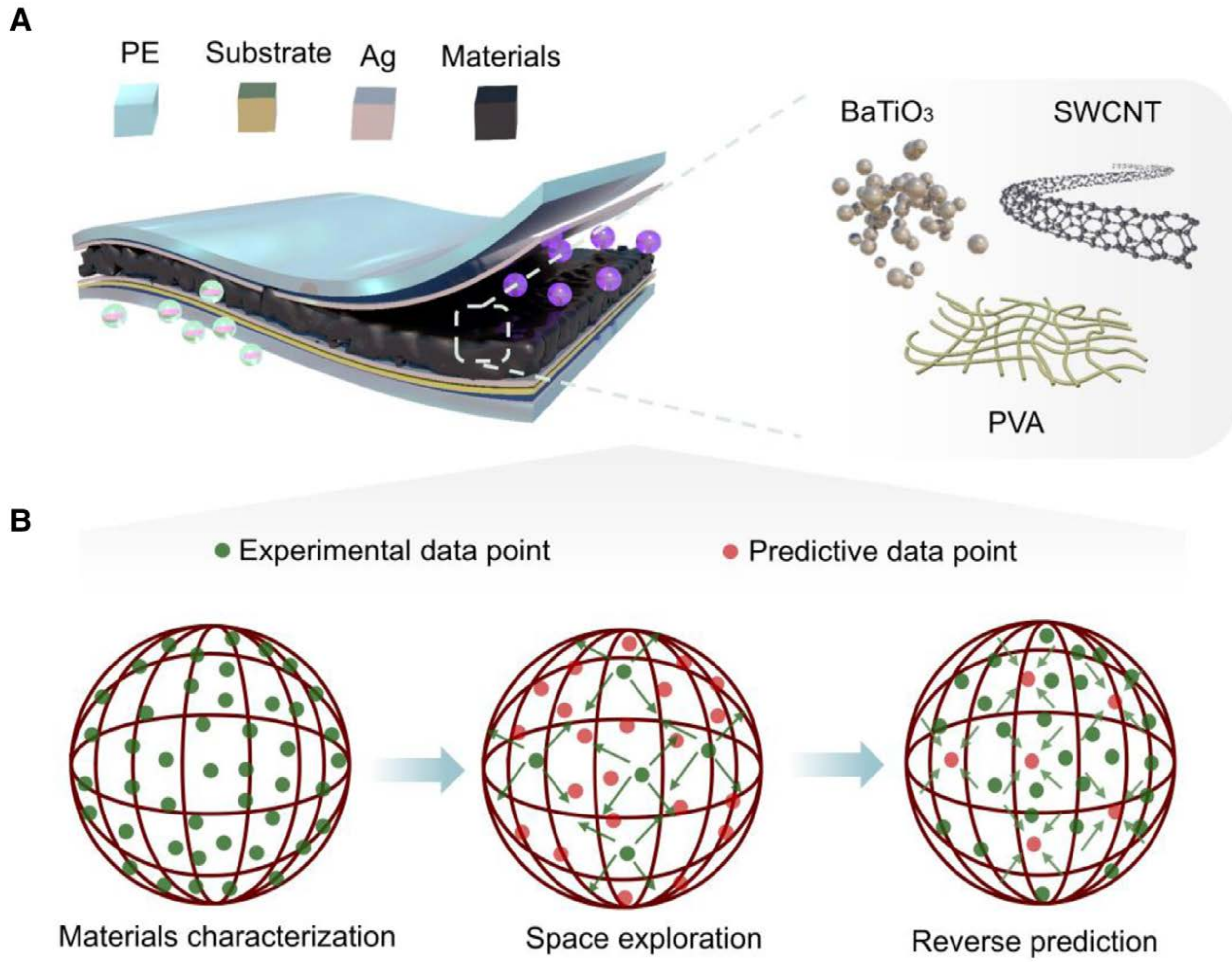

Figure 1. Automatic synthesis system of piezoelectric material. (A) Nanocomposite piezoelectric materials were prepared from 3 typical materials, PVA, SWCNT, and $BaTiO_3$. (B) The automatic synthesis of piezoelectric materials comprises 3 stages, materials characterization, space exploration, and reverse design.

successful material assembly. Elemental analysis of the pbs-PE material was performed by energy dispersive spectrometer (EDS) (Figure 2C and Supplementary Figure 2, http://links.lww.com/MEDMAT/A2), displaying a homogeneous distribution of elements such as Ba, Ti, O, and C. To further demonstrate that the 3 materials were well assembled, XPS tests were performed on both of the individual materials and pbs-PE material (Figure 2D and Supplementary Figure 3, http://links.lww.com/MEDMAT/A2). The energy spectrum exhibits characteristic peaks corresponding to Ba 3d, O 1s, Ti 2p, and C 1s. Additionally, the Raman spectra in Figure 2E substantiate the promising integration of PVA, $BaTiO_3$, and SWCNT components.

3.2 Space exploration via active learning

In this study, we introduce 2 parameters aimed at evaluating the sample characteristics of sample throughout the experimental process: charge-change ($\Delta Q/Q_0$) and maximum tensile strain (ε_{max}). The charge-change is defined by equation (4):

$$\frac{\Delta Q}{Q_0} = \frac{(Q_i - Q_0)}{Q_0} \tag{4}$$

where Q_i represents the peak–peak charge under different positive pressures and Q_0 is defined as the peak–peak charge under initial pressure 0.5 N. In addition, the maximum tensile strain was described in Note S1.

During the stage of design space exploration, we constructed an active learning loop model, illustrated in Figure 3A. First, all fabrication recipes (the distribution of fabrication recipes is shown in Figure 3B) yield 300 samples. Subsequently, characterize the characteristics of each sample, including piezoelectric transfer charge-changes and maximum tensile strain. For each sample, the peak–peak charge under 3 different pressures (0.5 N, 2 N, and 5 N) was identified, denoted as the corresponding peak–peak charges Q_1 for 2 N, and Q_2 for 5 N, and 2 charge-change values were calculated by equation (4) to serve as a charge-change label. Finally, 2 recipe labels (PVA loading and SWCNT loading), 2 charge-change labels ($\Delta Q_1/Q_0$, $\Delta Q_2/Q_0$), and maximum strain labels (ε_{max}) are integrated into an input data point for the active learning loop model, recording a total of 300 data points (Supplementary Table 1, http://links.lww.com/MEDMAT/A2).

To explore the design space, we inputted 300 data points into the active learning loop model. The model consists of 3 nonlinear algorithms: DT, KNN, and RF, as detailed in Note S2 for specific model construction. The training set constitutes 80% of the data points, while the remaining 20% comprises the test set, enabling the separate training of the 3 decision programs. Through iterative parameter adjustments, optimal training outcomes were obtained for each decision program. To assess the unfamiliarity level of the active learning model with the design space, the acquisition function based on 3 nonlinear algorithms is defined in equation (5):

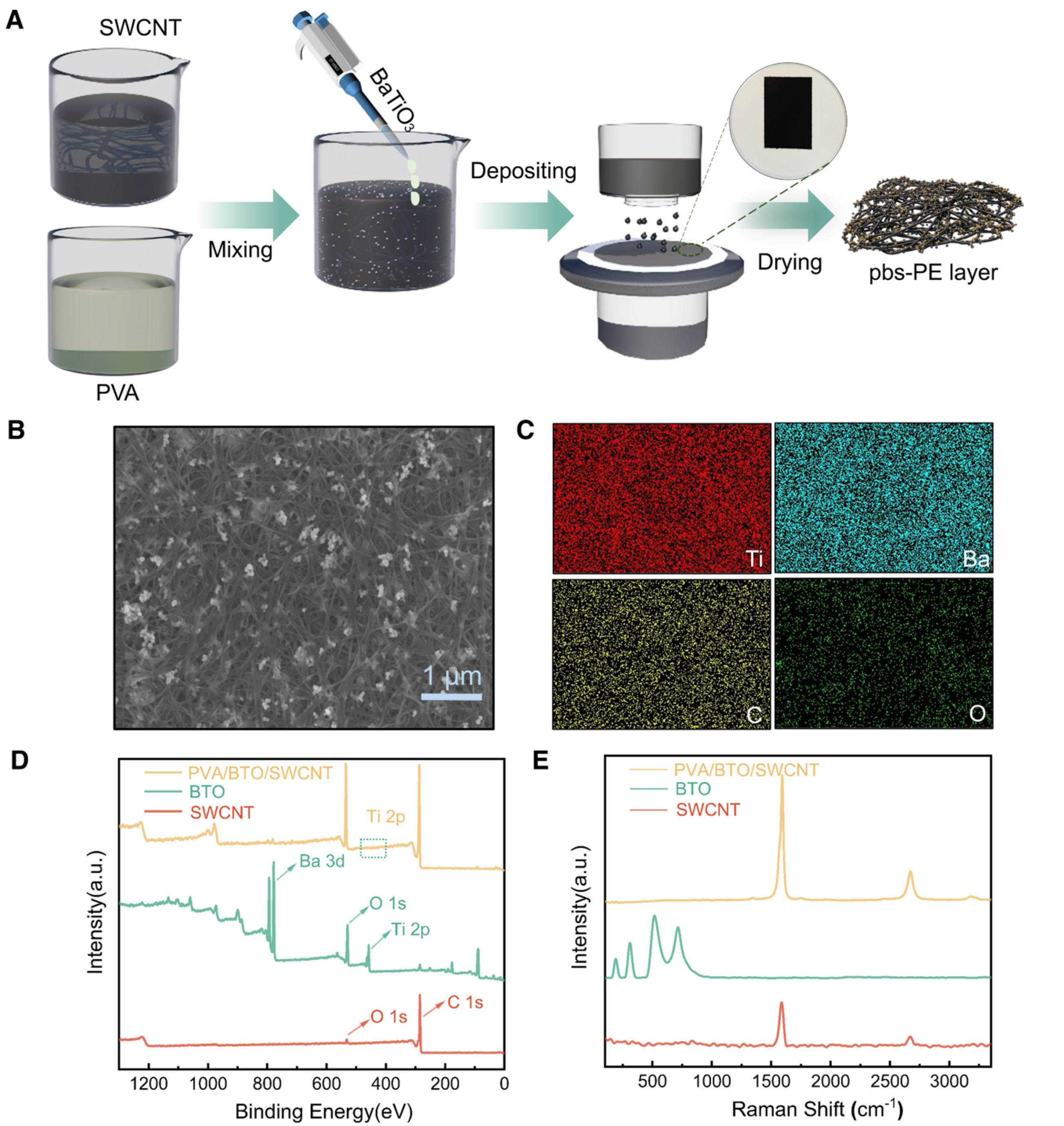

Figure 2. Preparation process and characterization diagram of pbs-PE material (PVA/SWCNT/ $BaTiO_3$ mass ratio is 20/45/35). (A) PVA/SWCNT/$BaTiO_3$ nanocomposite piezoelectric material is prepared through the mixing of PVA, SWCNT, and $BaTiO_3$ solutions, filtration, and drying. (B) SEM image of the surface morphology of the pbs-PE material. (C) EDS spectra of Ti, Ba, C, and O in the pbs-PE material. (D) XPS spectra of SWCNT, $BaTiO_3$, and pbs-PE materials. (E) Raman spectra of SWCNT, $BaTiO_3$, and pbs-PE materials.

$$\text{A-score} = L_2 \times \widehat{\sigma^2} \tag{5}$$

where L_2 represents the nearest mathematical distance between the current recipe label and the target recipe label and $\widehat{\sigma^2}$ represents the variance of the predicted label from the 3 decision procedures (detailed calculations of A-score are provided in Note S3). By calculating the A-score value for each input data point, we select the candidate with the highest A-score recommended by the active learning loop model. The target data point situated farthest from the current data point is selected, leading to further exploration of the design space.

However, significant uncertainty in the candidate with the highest A-score value is recommended by the model. In order to enhance the model's effectiveness in training these candidates, we collected the recommended recipes and labels for each loop. Subsequently, we generated novel samples through experiments and assessed the actual labels ($\Delta Q_1/Q_0$, $\Delta Q_2/Q_0$, and ε_{max}). Then added these data points into the original dataset, constituting a novel dataset for the subsequent active learning loop. The initial loop involved the collection of 10 data points. Following training with this updated dataset, the design space was further explored, and the model calculated

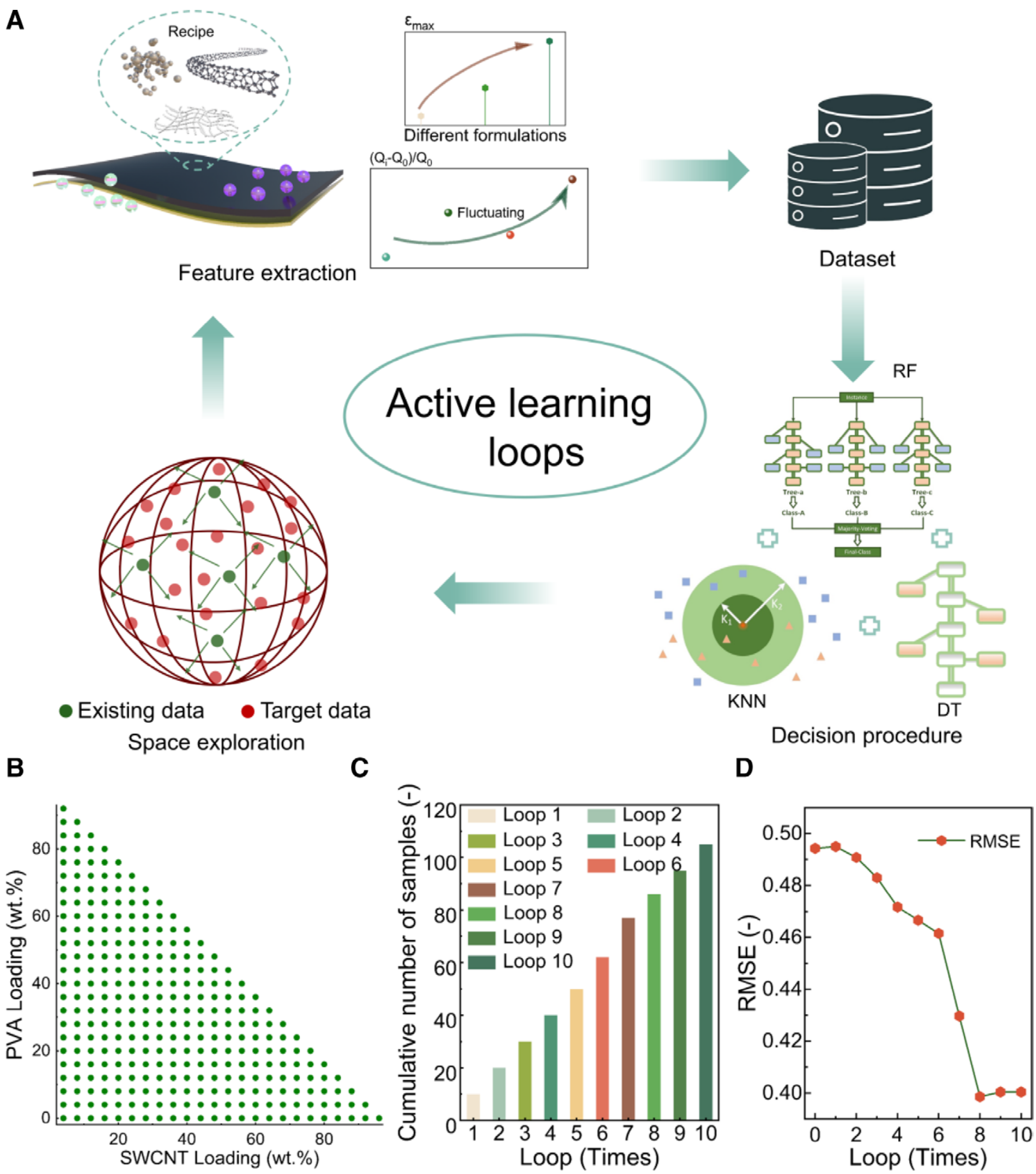

Figure 3. Spatial exploration process of sample design based on active learning. (A) The automatic material synthesis model is constructed through an active learning loop, including feature extraction (recipe, charge-change, and maximum tensile strain), data set construction, decision program construction (3 nonlinear algorithms RF, KNN, and DT), and data search. (B) Map of 300 different sample fabrication recipes, where the step of PVA and SWCNT loading change is set to 4%. (C) Cumulative number of samples manufactured in each active learning loop phase. (D) The trend of RMSE value changes during the active learning loop optimization process. (-) indicates that the parameter is dimensionless.

the A-score. Similarly, data points recommended by the model with the highest A-score were selected and subjected to experimental testing. By iteratively combining experiments with active learning loops to optimize the dataset, the design space is constantly explored. In the experiment, a total of 10 active learning loops were performed, and 105 samples were collected and tested. Figure 3C shows the cumulative number of samples after each active learning loop, while Supplementary Table 2, http://links.lww.com/MEDMAT/A2 details the sample recipe, charge-change, and maximum tensile strain label for each loop.

In this study, the active learning loop model continually evolves in its exploration of the design space and prediction accuracy. The predictive accuracy of the 3 decision programs was evaluated using the preprepared test set of 60 points. The trained model predicts labels from the test set data, including

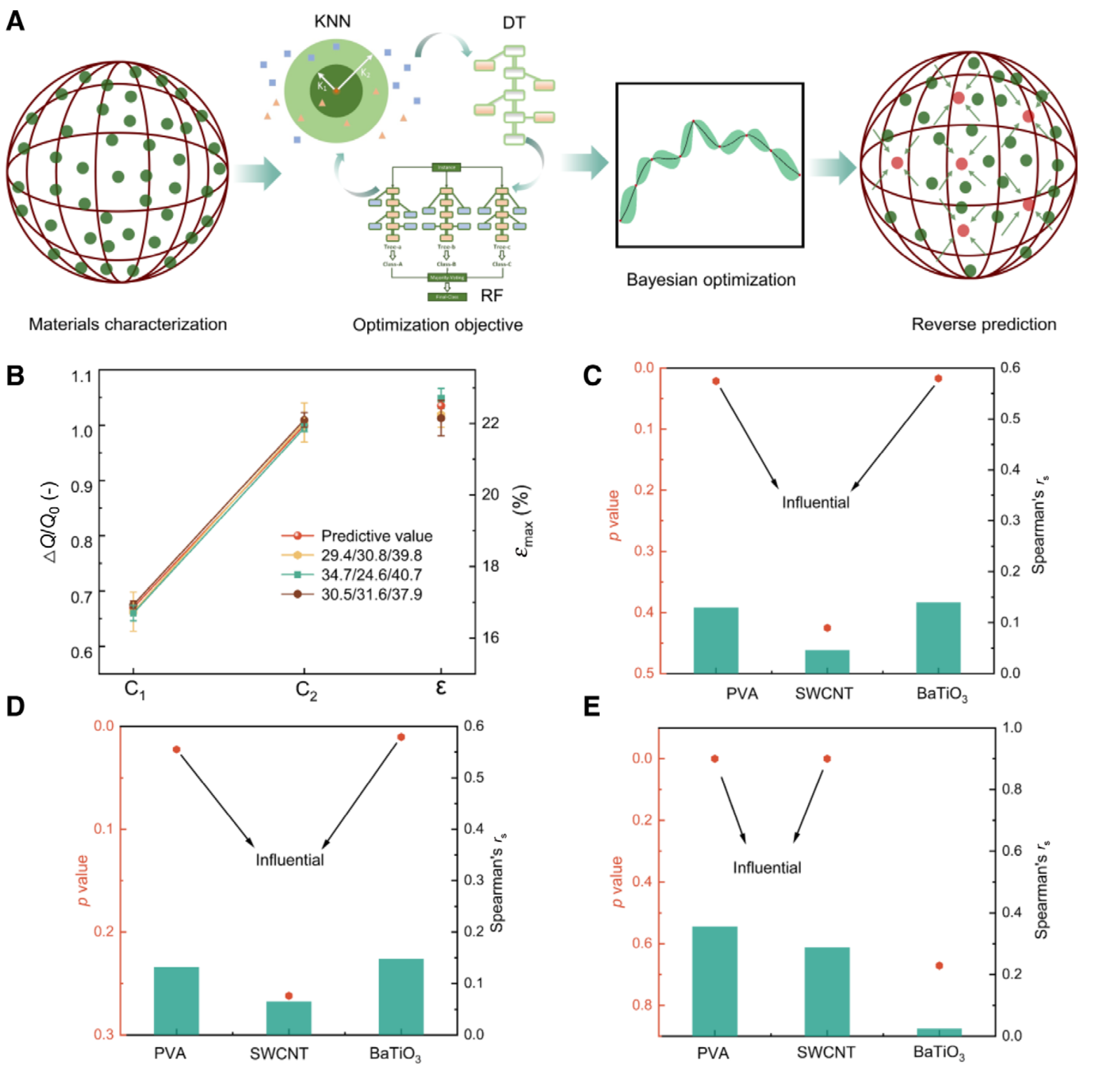

Figure 4. Reverse design model using Bayesian optimization and statistical analysis. (A) Reverse design flowchart through Bayesian optimization. (B) Comparison between the predicted value and actual value in the final reverse design model. Statistical analysis of the Spearman rank correlation coefficient between the sample recipe loading (PVA loading, SWCNT loading, and $BaTiO_3$ loading) and $\Delta Q_1/Q_0$, $\Delta Q_2/Q_0$, and ε_{max}, (C) $\Delta Q_1/Q_0$, (D) $\Delta Q_2/Q_0$, and (E) ε_{max}.

$\Delta Q_1/Q_0$, $\Delta Q_2/Q_0$, and ε_{max}. These predicted labels were then compared with the actual values of the test set data to calculate the RMSE, as defined in methods (refer to Note S4 for detailed instructions). The larger the RMSE, the lower the model prediction accuracy, and vice versa.

Figure 3D illustrates that the RMSE of the initial active learning loop model is relatively high, approximately 0.494. From the second to eighth loop, the increase in sample data enhances familiarity with the design space, leading to a consistent decline in RMSE. By the eighth loop, the RMSE reached approximately 0.398, which decreased by ~19.4% from the initial. After the eighth loop, RMSE basically stabilized at ~0.4. Via 10 loops, RMSE remained stable, and the model could basically predict the piezoelectric properties of PVA, SWCNT, and $BaTiO_3$ nanocomposite materials (Supplementary Figure 4, http://links.lww.com/MEDMAT/A2 also shows the RMSE trends of the three decision procedures in each stage of the 10-round active learning loop). On this basis, we also realize the reverse prediction of the recipe through the label.

3.3 Reverse design based on Bayesian optimization and correlation analysis

The reverse design model is used to formulate the sample fabrication recipe for the user-specified performance, as illustrated in Figure 4A. Initially, the design space and boundaries are established based on 300 initial samples and 105 samples generated through the active learning loop. Subsequently, 3 decision models from the final round of the active learning model are integrated into the optimization objective program. By amalgamating these decision models with performance metrics and

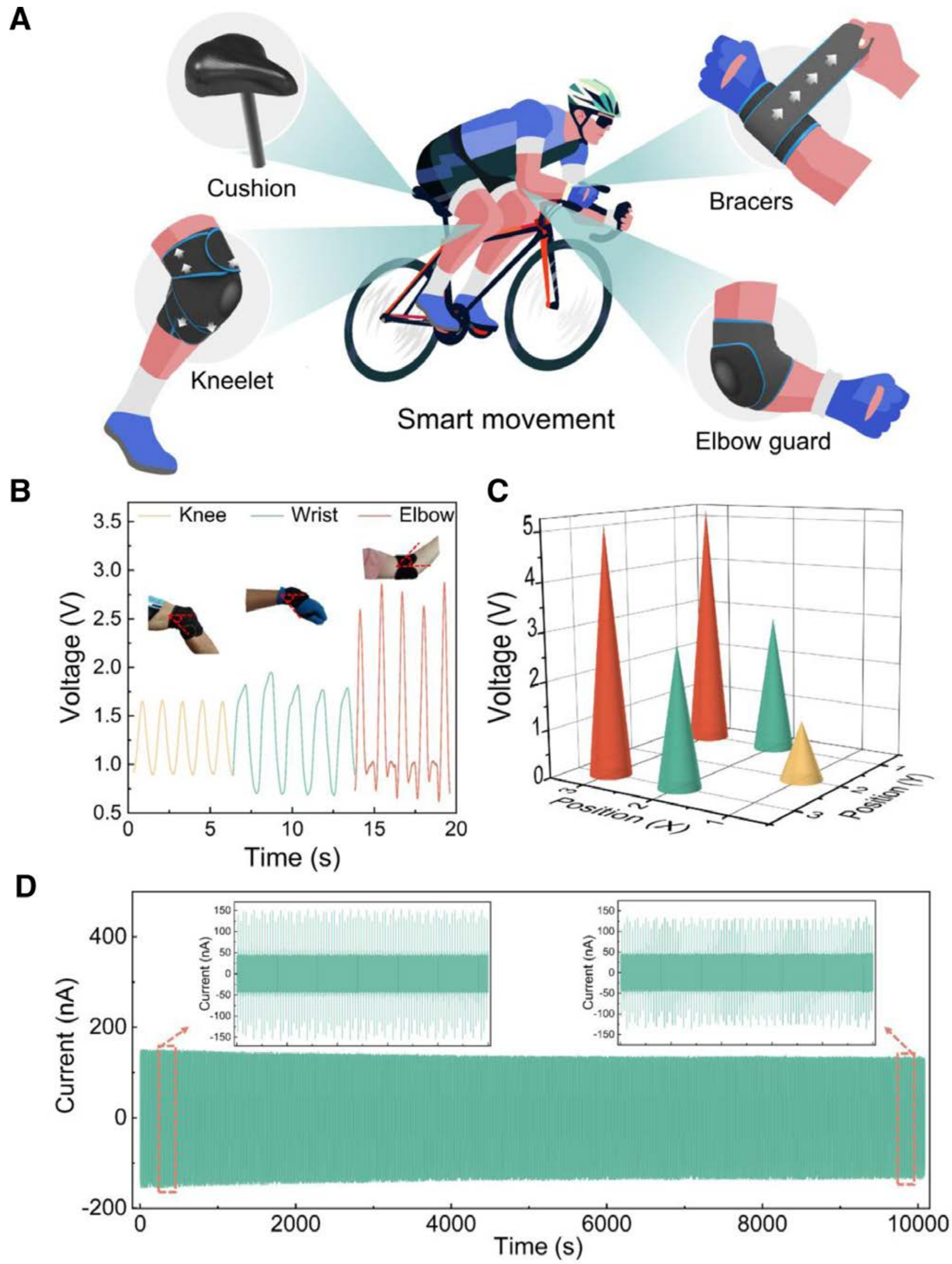

Figure 5. Application of sensors based on piezoelectric nanogenerators as flexible wearable devices. (A) Smart movement with PENG sensor, attaching to human joints (knees, wrists, elbows, etc.) and sports equipment (such as cushions) for energy collection and sensing. (B) The output voltage of different joints in the human body when bending 45°. (C) The maximum output voltage of the sensor array on the cushion while riding in an upright sitting position. (D) Mechanical durability.

search space, we define a loss function using MSE to evaluate the difference between target performance and predicted performance. To minimize the loss function, we employ the EI strategy within the Bayesian optimization algorithm (refer to methods) to explore the optimal combination of features in a given design space.

Then, we established the performance indicators as $\Delta Q_1/Q_0 = 0.67$, $\Delta Q_2/Q_0 = 1$, and $\varepsilon_{max} = 22.5\%$ for testing the accuracy of the reverse prediction model. We sorted the search results according to the loss function and selected the 3 groups of recipes with the smallest scores as feasible fabrication recipes (Supplementary Table 3, http://links.lww.com/MEDMAT/A2 provides 3 predicted recipes). These recipes were then used to produce samples for performance comparison. As depicted in Figure 4B, the deviation between the predicted recipes' performance and the actual performance indices is minimal, which indicates that the reverse prediction model is relatively accurate in predicting the charge-change and maximum strain.

In the experiment, samples were fabricated using various material recipes, and peak–peak charge-changes and maximum tensile strain were measured under varying pressures. However, there is a nonlinear relationship between the material recipe and its properties, which cannot be obtained by simple observation. Therefore, in order to reveal this connection and search for reliable rules for material synthesis, Spearman rank correlation coefficient (Spearman r_s)[37] and P values[30] are introduced (Spearman rank correlation coefficient and P values are detailed in Note S5).

Here, we examine the correlation between the material recipe and $\Delta Q_1/Q_0$. As shown in Figure 4C, the Spearman r_s corresponding to $BaTiO_3$ and PVA is larger and the corresponding P value is smaller, while the Spearman r_s corresponding to SWCNT is smallest and the P value is largest. This indicates that the influence of $BaTiO_3$ and PVA on charge-change is greater than that of SWCNT. Figure 4D shows the correlation between the material recipe and $\Delta Q_2/Q_0$, and the results are consistent with Figure 4C, which again proves the above conclusion. In addition, we also analyzed the nonlinear correlation between the material recipe and the ε_{max} of the pbs-PE material. As shown in Figure 4E, PVA and SWCNT have almost the same influence on ε_{max}, and the influence is larger, while $BaTiO_3$ has the least effect.

3.4 Health exercise monitoring

Here, the motion sensing of PENG based on the pbs-PE material is discussed. Due to pbs-PE-based PENG demonstrating exceptional mechanical durability and flexibility, these properties render it promising for applications in flexible wearable health motion sensors, particularly those designed for seamless integration onto human joints and motion devices (Figure 5A). In the experiment, we use the reverse prediction model to recommend a feasible recipe (~30%) of the estimated maximum tensile strain. Figure 5B, Supplementary Figure 5, http://links.lww.com/MEDMAT/A2, and Supplementary Movie 1, http://links.lww.com/MEDMAT/A3 show the motion monitoring feedback when the PENG sensor is installed at the joint and bent at 45°. Supplementary Figures 6 and 7, http://links.lww.com/MEDMAT/A2, and Supplementary Movie 2, http://links.lww.com/MEDMAT/A4 show the signal feedback of each joint bending at 90°. Remarkably, distinct electrical signals were observed for different joints bending at the same angle, showing the potential of joint posture monitoring.

As shown in Supplementary Figure 8, http://links.lww.com/MEDMAT/A2, we also integrated multiple PENG sensors into the bike seat cushion to form an array of piezoelectric sensors. By affixing 5 PENG sensors on the seat cushion, the output signal of each sensor under different riding postures can be monitored in real time. Figure 5C shows the maximum output voltage of each sensor under the upright sitting. Notably, sensor-4 and sensor-5 yielded the highest output (~5.2 V), whereas sensor-1 produced the lowest output (~1.2 V). At the same time, signals from different sitting positions were monitored and analyzed by COMSOL Multiphysics simulation (Supplementary Figures 9–12, http://links.lww.com/MEDMAT/A2 and Supplementary Movie 3, http://links.lww.com/MEDMAT/A5). The results revealed distinctive outputs from various sensors corresponding to different sitting positions. This variance presents a valuable means for real-time movement status monitoring, offering potential applications in guiding cycling and other physical activities for enhanced health.

Finally, we also tested the mechanical durability of PENG sensor, as shown in Figure 5D. After continuous operation for 10,000 s, the sensor still maintains stable output performance, which enables it to be used for long-term monitoring.

4. Conclusions

In summary, we report a composite material synthesis method that combines experiments with ML algorithms. This approach can achieve performance prediction of multiple material composites. We selected 3 typical materials (PVA, SWCNT, and $BaTiO_3$) to produce 300 samples. Through a closed-loop active learning model primarily constructed by nonlinear algorithms (DT, KNN, and RF), the design space is explored and the dataset is optimized. After 10 learning loops, 105 samples were fabricated, with an error reduction of 19.4% compared to the initial test. Additionally, the reverse prediction model based on Bayesian optimization was trained with 405 samples to recommend feasible sample recipes according to the user's needs. Correlation analysis was used to further investigate the rules of material synthesis, revealing the effects of 3 materials on the performance of the composite piezoelectric material. Finally, the reverse prediction model was used to recommend the sensor recipe suitable for health exercise monitoring, and the real-time monitoring of human joints and exercise equipment was realized. This work is expected to accelerate material synthesis and has great potential in realizing intelligent movement.

Funding

This research was supported by the National Natural Science Foundation of China (No. 52192610) and National Key R & D Project from Minister of Science and Technology (No. 2020YFC2005800).

Conflicts of interests

The authors declare that they have no conflicts of interest.

Data availability

Data will be made available on request.

Author contributions

W.T. initiated and directed the project. E.Z. fabricated the devices. E.Z., T.W., Y.W., F.Z., L.C., and Z.Z. performed measurements and analyzed the data. E.Z., T.W., and W.T. wrote the manuscript. All authors contributed to discussions.

References

[1] Rus D, Tolley MT. Design, fabrication and control of soft robots. *Nature*. 2015;521(7553):467–475.
[2] Cooper CB, Root SE, Michalek L, et al. Autonomous alignment and healing in multilayer soft electronics using immiscible dynamic polymers. *Science*. 2023;380(6648):935–941.
[3] Lee Y, Koehler F, Dillon T, et al. Magnetically actuated fiber-based soft robotsarticle; early access. *Adv Mater*. 2023;2023:e2301916.
[4] Fischer P, Nelson BJ, Yang GZ. New materials for next-generation robots. *Sci Robot*. 2018;3:eaau0448.
[5] Laschi C, Mazzolai B, Cianchetti M. Soft robotics: technologies and systems pushing the boundaries of robot abilities. *Sci Robot*. 2016;1:eaah3690.
[6] Sheiko SS, Everhart MH, Dobrynin AV, et al. Encoding tissue mechanics in silicone. *Sci Robot*. 2018;3:eaat7175.
[7] Sinar D, Knopf GK. Disposable piezoelectric vibration sensors with PDMS/ZnO transducers on printed graphene-cellulose electrodes. *Sens Actuators A*. 2020;302:111800.
[8] Park KI, Jeong CK, Ryu J, et al. Flexible and large-area nanocomposite generators based on lead zirconate titanate particles and carbon nanotubes. *Adv Energy Mater*. 2013;3(12):1539–1544.
[9] Yan JH, Han YH, Xia SH, et al. Polymer template synthesis of flexible BaTiO3 crystal nanofibers. *Adv Funct Mater*. 2019;29(51):1907919.
[10] Qian YT, Kangg DJ. Poly(dimethylsiloxane)/ZnO nanoflakes/three-dimensional graphene heterostructures for high-performance flexible

energy harvesters with simultaneous piezoelectric and triboelectric generation. *ACS Appl Mater Interfaces*. 2018;10(38):32281–32288.

[11] Meisak D, Kinka M, Plyushch A, et al. Piezoelectric nanogenerators based on BaTiO3/PDMS composites for high-frequency applications. *ACS Omega*. 2023;8(15):13911–13919.

[12] Wang M, Hou XJ, Qian S, et al. An intelligent glove of synergistically enhanced ZnO/PAN-based piezoelectric sensors for diversified human-machine interaction applications. *Electronics*. 2023;12(8):1782.

[13] D'Ambrogio G, Zahhaf O, Bordet M, et al. Structuring BaTiO3/PDMS nanocomposite via dielectrophoresis for fractional flow reserve measurement. *Adv Eng Mater*. 2021;23(10):2100341.

[14] You YM, Liao WQ, Zhao DW, et al. An organic-inorganic perovskite ferroelectric with large piezoelectric response. *Science*. 2017;357(6348):306–309.

[15] Deng W, Zhou Y, Libanori A, et al. Piezoelectric nanogenerators for personalized healthcare. *Chem Soc Rev*. 2022;51(9):3380–3435.

[16] Su Y, Li W, Yuan L, et al. Piezoelectric fiber composites with polydopamine interfacial layer for self-powered wearable biomonitoring. *Nano Energy*. 2021;89:106321.

[17] Su Y, Chen C, Pan H, et al. Muscle fibers inspired high-performance piezoelectric textiles for wearable physiological monitoring. *Adv Funct Mater*. 2021;31(19):2010962.

[18] Libanori A, Chen G, Zhao X, et al. Smart textiles for personalized healthcare. *Nat Electron*. 2022;5(3):142–156.

[19] Raccuglia P, Elbert KC, Adler PDF, et al. Machine-learning-assisted materials discovery using failed experiments. *Nature*. 2016;533(7601):73–76.

[20] Jiao PC. Emerging artificial intelligence in piezoelectric and triboelectric nanogenerators. *Nano Energy*. 2021;88(21):106227.

[21] Lookman T, Balachandran PV, Xue DZ, et al. Active learning in materials science with emphasis on adaptive sampling using uncertainties for targeted design. *npj Comput Mater*. 2019;5:17.

[22] Kusne AG, Yu HS, Wu CM, et al. On-the-fly closed-loop materials discovery via Bayesian active learning. *Nat Commun*. 2020;11(1):5966.

[23] Wang YQ, Liu XZ, Zheng ZH, et al. Numerical analysis and structural optimization of cylindrical grating-structured triboelectric nanogenerator. *Nano Energy*. 2021;90:106570.

[24] Jiao PC, Alavi AH. Artificial intelligence-enabled smart mechanical metamaterials: advent and future trends. *Int Mater Rev*. 2021;66(6):365–393.

[25] Jing HR, Guan CH, Yang Y, et al. Machine learning-assisted design of AlN-based high-performance piezoelectric materials. *J Mater Chem A*. 2023;11(27):14840–14849.

[26] Muraoka K, Sada Y, Miyazaki D, et al. Linking synthesis and structure descriptors from a large collection of synthetic records of zeolite materials. *Nat Commun*. 2019;10:4459.

[27] Schmidt J, Marques MRG, Botti S, et al. Recent advances and applications of machine learning in solid-state materials science. *npj Comput Mater*. 2019;5:36.

[28] Bassman L, Rajak P, Kalia RK, et al. Active learning for accelerated design of layered materials. *npj Comput Mater*. 2018;4:9.

[29] Williams T, McCullough K, Lauterbach JA. Enabling catalyst discovery through machine learning and high-throughput experimentation. *Chem Mat*. 2020;32(1):157–165.

[30] Yang HT, Li JL, Lim KZ, et al. Automatic strain sensor design via active learning and data augmentation for soft machines. *Nat Mach Intell*. 2022;4(1):84–94.

[31] Liu YT, Kelley KP, Vasudevan RK, et al. Experimental discovery of structure-property relationships in ferroelectric materials via active learning. *Nat Mach Intell*. 2022;4(4):341–350.

[32] Ament S, Amsler M, Sutherland DR, et al. Autonomous materials synthesis via hierarchical active learning of nonequilibrium phase diagrams. *Sci Adv*. 2021;7(51):eabg4930.

[33] Epps RW, Bowen MS, Volk AA, et al. Artificial chemist: an autonomous quantum dot synthesis bot. *Adv Mater*. 2020;32(30):e2001626.

[34] MacLeod BP, Parlane FGL, Morrissey TD, et al. Self-driving laboratory for accelerated discovery of thin-film materials. *Sci Adv*. 2020;6(20):eaaz8867.

[35] Zhang JQ, Tian HR, Wang PX, et al. Improving wheat yield estimates using data augmentation models and remotely sensed biophysical indices within deep neural networks in the Guanzhong Plain, PR China. *Comput Electron Agric*. 2022;192:13.

[36] Hansen TM, Stavem K, Rand K. Sample size and model prediction accuracy in EQ-5D-5L valuations studies: expected out-of-sample accuracy based on resampling with different sample sizes and alternative model specifications. *MDM Policy Pract*. 2022;7(1):23814683221083839.

[37] Schober P, Boer C, Schwarte LA. Correlation coefficients: appropriate use and interpretation. *Anesth Analg*. 2018;126(5):1763–1768.

How to cite this article: Zhao E, Wang T, Wang Y, Zeng F, Chen L, Zhu Z, Tang W. Active learning assisted piezoelectric materials synthesis on the basis of composite decision-making. MedMat 2024;1(2):e00006. doi: 10.1097/mm9.0000000000000006